

# High-Frequency Nonlinearity Analysis of Common-Emitter and Differential-Pair Transconductance Stages

Keng Leong Fong, *Member, IEEE*, and Robert G. Meyer, *Fellow, IEEE*

**Abstract**—Equations describing the high-frequency nonlinear behavior of common-emitter and differential-pair transconductance stages are derived. The equations show that transconductance stages using inductive degeneration are more linear than those using capacitive or resistive degeneration, and that the common-emitter transconductance stages are more linear than the differential-pair transconductance stages with the same bias current and transconductance. The nonlinearity equations can also be used to explain the class AB behavior of the common-emitter transconductance stage with inductive degeneration.

**Index Terms**—Amplifier distortion, analog integrated circuits, circuit analysis, circuit optimization, nonlinear circuits, nonlinear distortion, nonlinear equations, Volterra series.

## I. INTRODUCTION

THE rapid growth of portable wireless communication systems has led to a demand for low-power, high-performance, and highly integrated RF circuits. The bipolar-transistor common-emitter and differential-pair transconductance stages shown in Figs. 1 and 2, respectively, are commonly used in many radio frequency (RF) building blocks, such as low-noise amplifiers (LNA) and mixers. To improve the linearity, the transconductance stages are usually degenerated by impedance  $Z_e$ , which can be implemented by using either resistors, capacitors, or inductors. It is easily shown that transconductance stages with reactive (inductive or capacitive) degeneration have lower noise figure (NF) than those with resistive degeneration since the degeneration reactance (apart from its loss resistance) does not introduce an additional noise source. Similarly, differential-pair transconductance stages have a higher noise figure than common-emitter transconductance stages since the former have more noise generators. However, there is little published information about linearity comparisons among resistive, capacitive, and inductive degeneration, and between common-emitter and differential-pair transconductance stages.

Manuscript received April 7, 1997; revised August 28, 1997. This material is based on work supported in part by the U.S. Army Research Office under Grant DAAH04-93-F-0200.

K. L. Fong was with the Electronics Research Laboratory, Department of Electrical Engineering and Computer Science, University of California, Berkeley, CA 94720-1772 USA. He is now with Philips Semiconductors, Sunnyvale, CA 94088-3409 USA.

R. G. Meyer is with the Electronics Research Laboratory, Department of Electrical Engineering and Computer Science, University of California, Berkeley, CA 94720-1772 USA.

Publisher Item Identifier S 0018-9200(98)02326-9.

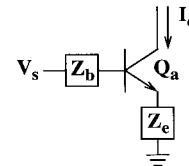


Fig. 1. Common-emitter transconductance stage.

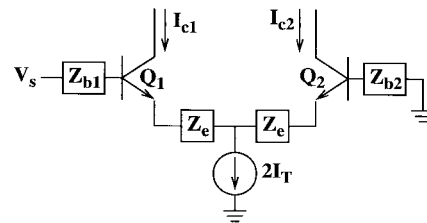


Fig. 2. Differential-pair transconductance stage.

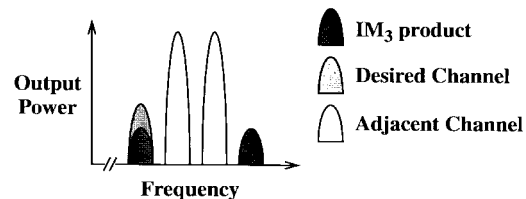


Fig. 3. Third-order intermodulation product corrupts desired channel.

In this paper, high-frequency nonlinearity equations in Volterra series [1], [2] for both common-emitter and differential-pair transconductance stages are derived. The emphasis is on interpretation and application of the equations. The nonlinearity equations are also used to explain the class AB behavior described in [3] and [4].

## II. THIRD-ORDER INTERMODULATION DISTORTION

Due to the third-order nonlinearity of a transconductance stage, two undesired signals in adjacent channels generate third-order intermodulation ( $IM_3$ ) products at the output of the transconductance stage. As illustrated in Fig. 3, the  $IM_3$  product can corrupt the desired signal if it falls within the desired channel. If the two adjacent channel frequencies are  $\omega_a$  and  $\omega_b$ , respectively, two  $IM_3$  products are generated at frequencies  $(2\omega_a - \omega_b)$  and  $(2\omega_b - \omega_a)$ , respectively.

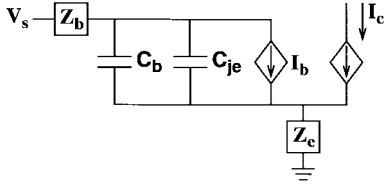


Fig. 4. Model of common-emitter transconductance stage.

Fig. 4 shows the large-signal model used to derive the non-linearity equations for the common-emitter transconductance stage shown in Fig. 1. This model ignores the effect of base-collector junction capacitance ( $C_\mu$ ) of  $Q_a$ . Inclusion of  $C_\mu$  greatly complicates the analysis without adding significant accuracy to the results in typical situations.  $V_s$  is the voltage signal source.  $Z_b$  is the impedance at the base of  $Q_a$  which includes source resistance ( $R_s$ ), base resistance ( $r_b$ ) of  $Q_a$ , shunt impedance of bias circuit, and impedance of impedance-matching network.  $Z_e$  is the impedance at the emitter of  $Q_a$  which includes the parasitic emitter resistance ( $r_e$ ) of  $Q_a$  and the impedance of the degeneration elements (resistor, capacitor, and/or inductor).  $C_b$  is the base-charging capacitance of  $Q_a$  which is linearly proportional to the collector current ( $I_c$ ) and the forward transit time ( $\tau_F$ ) of  $Q_a$ .  $C_{j_e}$  is the base-emitter junction capacitance which is assumed to be constant in this model.  $I_b$  is the base current which is equal to  $I_c/\beta_0$  where  $\beta_0$  is the small-signal low-frequency current gain of  $Q_a$ .  $I_b$  cannot be ignored since the high-frequency nonlinearity also depends on the low-frequency characteristics of  $Q_a$  (this will become obvious later). Using the model in Fig. 4, a Kirchhoff's voltage law equation can be written as

$$V_s = (sC_{j_e}V_\pi + s\tau_F I_c + I_c/\beta_0)(Z_b + Z_e) + I_c Z_e + V_\pi \quad (1)$$

where  $I_c$  is the collector signal current (collector current minus bias current) where the collector is assumed to be ac grounded,  $V_\pi$  is the base-emitter signal voltage drop across  $C_b$  and  $C_{j_e}$ , and  $s(=j\omega)$  is the Laplace variable. Solving this equation (derivation is shown in Appendix A) results in the following Volterra series expression:

$$I_c = A_1(s) \circ V_s + A_2(s_1, s_2) \circ V_s^2 + A_3(s_1, s_2, s_3) \circ V_s^3 + \dots \quad (2)$$

where  $V_s^n$  is the  $n$ th power of the voltage source signal and  $A_n(\cdot)$  is the Volterra series coefficient which is a linear function of  $n$  number of frequencies. The operator "o" indicates multiplying each frequency component in  $V_s^n$  by the magnitude of  $A_n(\cdot)$  and shifting each frequency component in  $V_s^n$  by the

phase of  $A_n(\cdot)$ . The first three Volterra series coefficients are

$$A_1(s) = \frac{g_m}{[sC_{j_e}Z(s) + s\tau_F g_m Z(s) + g_m Z(s)/\beta_0 + 1 + g_m Z_e(s)]} \quad (3)$$

$$A_2(s_1, s_2) = A_1(s_1 + s_2)A_1(s_1)A_1(s_2) \frac{V_T}{2I_Q^2} \times [1 + (s_1 + s_2)C_{j_e}Z(s_1 + s_2)] \quad (4)$$

$$A_3(s_1, s_2, s_3) = A_1(s_1 + s_2 + s_3) \frac{V_T}{3I_Q^3} \times [-A_1(s_1)A_1(s_2)A_1(s_3) + 3I_Q \overline{A_1 A_2}] \times [1 + (s_1 + s_2 + s_3)C_{j_e}Z(s_1 + s_2 + s_3)] \quad (5)$$

where  $Z(s)$ ,  $\overline{A_1 A_2}$ , and  $g_m$  are as shown in the equations at the bottom of the page,  $I_Q$  is the bias current of  $Q_a$ , and  $V_T$  is the thermal voltage. The coefficient  $A_1(s)$  is the small-signal transconductance of the transconductance stage.

The  $IM_3$  product at frequency ( $2\omega_a - \omega_b$ ) can be calculated by using the Volterra series coefficient  $A_3(s_1, s_2, s_3)$ , and letting  $s_1 = s_a$ ,  $s_2 = s_a$ , and  $s_3 = -s_b$ . Similarly, the  $IM_3$  product at frequency ( $2\omega_b - \omega_a$ ) can be calculated by letting  $s_1 = s_b$ ,  $s_2 = s_b$ , and  $s_3 = -s_a$ . Typically, the frequency difference between  $\omega_a$  and  $\omega_b$  is so small that  $s \approx s_a \approx s_b$  can be assumed. Using two input signals of the same amplitude  $V_s$ , the magnitude ( $|IM_3|$ ) of the input-referred  $IM_3$  products (the two  $IM_3$  products have about the same magnitude) of the common-emitter transconductance stage is given by

$$|IM_3| = \left| \frac{3}{4} \frac{A_3(s_a, s_a, -s_b)}{A_1(2s_a - s_b)} \right| |V_s|^2 \approx \left| \frac{A_1(s)}{I_Q} \right|^3 \left| \frac{V_T}{4} [1 + sC_{j_e}Z(s)] \times \left\{ -1 + \frac{A_1(\Delta s)}{g_m} [1 + \Delta s C_{j_e}Z(\Delta s)] + \frac{A_1(2s)}{2g_m} [1 + 2sC_{j_e}Z(2s)] \right\} \right| |V_s|^2 \quad (6)$$

where  $\Delta s = (s_a - s_b) \ll s$ .

The  $|IM_3|$  depends on the magnitude of

$$[1 + sC_{j_e}Z_b(s) + sC_{j_e}Z_e(s)]. \quad (7)$$

$$Z(s) = Z_b(s) + Z_e(s) \\ \frac{1}{A_1 A_2} = \frac{A_1(s_1)A_2(s_2, s_3) + A_1(s_2)A_2(s_1, s_3) + A_1(s_3)A_2(s_1, s_2)}{3} \\ g_m = \frac{I_Q}{V_T}$$

With inductive degeneration, the  $[sC_{je}Z_e(s)]$  term is a negative real number which cancels the “1” term in (7) partially. There is no such cancellation with resistive degeneration since the  $[sC_{je}Z_e(s)]$  term is a positive imaginary number which adds to the imaginary part of the  $[sC_{je}Z_b(s)]$  term in (7). For the same reason, capacitive degeneration would increase the  $|IM_3|$  because the  $[sC_{je}Z_e(s)]$  term is a positive real number which adds to the “1” term in (7).

The  $|IM_3|$  also depends on the magnitude of

$$\left\{ -1 + \frac{A_1(\Delta s)}{g_m} [1 + \Delta s C_{je} Z(\Delta s)] + \frac{A_1(2s)}{2g_m} [1 + 2s C_{je} Z(2s)] \right\} \quad (8)$$

where the “-1” and

$$\left\{ \frac{A_1(\Delta s)}{g_m} [1 + \Delta s C_{je} Z(\Delta s)] + \frac{A_1(2s)}{2g_m} [1 + 2s C_{je} Z(2s)] \right\}$$

terms come from the third-order nonlinearity ( $A_1 A_1 A_1$ ) and the second-order interaction ( $\overline{A_1 A_2}$ ), respectively. Using the following approximation (for practical design values),

$$[1 + \Delta s C_{je} Z(\Delta s)] \approx 1$$

equation (6) can be simplified to

$$|IM_3| \approx \left| \frac{A_1(s)}{I_Q} \right|^3 \left| \frac{V_T}{4} [1 + s C_{je} Z(s)] \times \left\{ -1 + \frac{A_1(\Delta s)}{g_m} + \frac{A_1(2s)}{2g_m} [1 + 2s C_{je} Z(2s)] \right\} \right| |V_s|^2 \quad (9)$$

where the value of the  $\left\{ \frac{A_1(2s)}{2g_m} [1 + 2s C_{je} Z(2s)] \right\}$  term is typically small, compared to the value of the  $[A_1(\Delta s)/g_m]$  term. However, it is not so small that it can be ignored.

As shown in (9), the  $|IM_3|$  is independent of  $\tau_F$  if the small-signal transconductance  $[A_1(s)]$  is kept constant. On the other hand, it increases with  $C_{je}$  for the resistive and capacitive degeneration cases since the  $[sC_{je}Z_e(s)]$  term is a positive imaginary number and a positive real number, respectively, but decreases with  $C_{je}$  for the inductive degeneration case because the  $[sC_{je}Z_e(s)]$  term is a negative real number. Furthermore, the  $|IM_3|$  is proportional to the cube of the ratio of small-signal transconductance to bias current ( $I_Q$ ).

The  $|IM_3|$  can be lowered by increasing the  $A_1(\Delta s)$  term. This increases the second-order interaction to cancel the third-order nonlinearity. Since the degeneration inductor has low impedance at low frequency, the  $A_1(\Delta s)$  term in the inductive degeneration case is much larger than those in the resistive and capacitive degeneration cases. Similarly, the degeneration capacitor has high impedance at low frequency, and hence the  $A_1(\Delta s)$  term in the capacitive degeneration case is much smaller than that in the resistive degeneration case. This is the second reason why the inductively degenerated transconductance stage is more linear than the resistively degenerated transconductance stage, which in turn is more linear than the capacitive degenerated transconductance stage with the same transconductance and bias current.

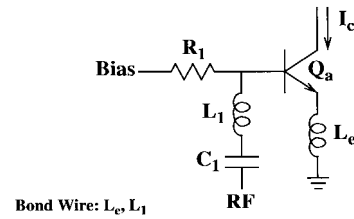


Fig. 5. Inductively degenerated common-emitter transconductances stage.

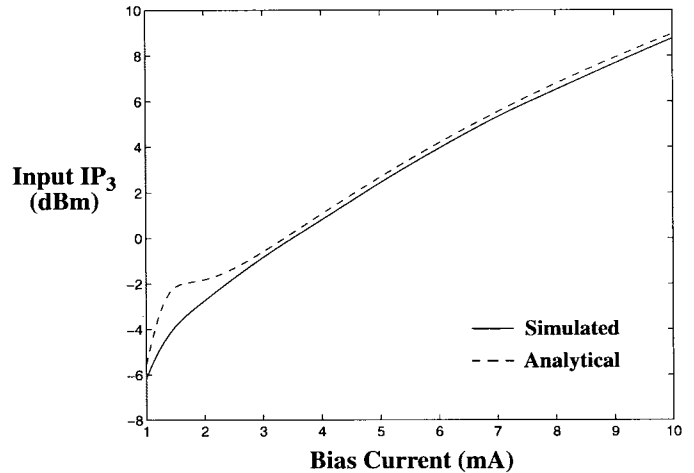


Fig. 6. Input  $IP_3$  versus bias current.

Fig. 5 shows the basic topology of a typical common-emitter transconductance stage with inductive degeneration. The degeneration inductor  $L_e$  is typically implemented by bond wires.  $C_1$  serves as a dc blocking capacitor. It is also used to tune out the bond wire inductance  $L_1$ .  $R_1$  is a bias resistor used to isolate the bias circuit from the RF port. At low frequency ( $\Delta s$ ), the impedance of  $Z_e(\Delta s) (\approx \Delta s L_e)$  is negligible. The impedance of  $Z_b(\Delta s)$  is dominated by the bias resistor  $R_1$  since the blocking capacitor  $C_1$  has high impedance at low frequency. In this case, the  $[A_1(\Delta s)/g_m]$  term in (9) can be simplified to

$$\frac{A_1(\Delta s)}{g_m} \approx \frac{r_\pi}{r_\pi + R_1} \quad (10)$$

where  $r_\pi$  is the small-signal base-emitter resistance of  $Q_a$ . Therefore, in order to increase the linearity,  $R_1$  should be kept small (relative to  $r_\pi$ ) to increase the second-order interaction. However,  $R_1$  has to be large enough to avoid significant loading on the RF port, which would cause impedance mismatch and noise figure degradation.

Fig. 6 shows the simulated (using HSPICE) and analytical [using (6)] input  $IP_3$  of the common-emitter transconductance stage shown in Fig. 5 as a function of bias current ( $I_Q$ ). The simulation results include the nonlinear effects of  $C_\mu$  and  $C_{je}$  of  $Q_a$ . Neglecting these effects does not seem to introduce significant errors. The two RF sinusoidal signals used are at 900 and 910 MHz, respectively. The component values used are:  $\tau_F = 10.5$  ps,  $C_{je} = 1.17$  pF,  $\beta = 73$ ,  $L_e = 2.4$  nH,  $L_1 = 3.5$  nH,  $C_1 = 20$  pF, and  $R_1 = 150 \Omega$ .

Similarly, the model shown in Fig. 7 is used to derive the nonlinearity equations for the differential-pair transduc-

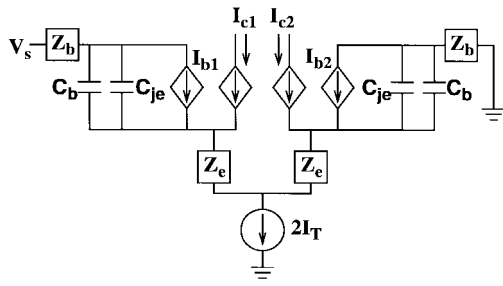


Fig. 7. Model of differential-pair transconductance stage.

tance stage shown in Fig. 2. This model ignores the effect of the base-collector junction capacitance ( $C_{\mu}$ ) of  $Q_1$  and  $Q_2$ . The base impedance ( $Z_{b1} + Z_{b2}$ ) in Fig. 2 is split into two  $Z_b$ 's in Fig. 7 to simplify the derivation by exploiting symmetry. There is no loss of generality in this manipulation if the tail current source ( $2I_T$ ) has infinite output impedance. Using the model in Fig. 7, Kirchhoff's voltage law and Kirchhoff's current law equations can be written as

$$\begin{aligned} V_s &= (sC_{je}V_{\pi 1} + s\tau_F I_{c1} + I_{c1}/\beta_0)(Z_b + Z_e) \\ &\quad + I_{c1}Z_e + V_{\pi 1} \\ &\quad - (sC_{je}V_{\pi 2} + s\tau_F I_{c2} + I_{c2}/\beta_0)(Z_b + Z_e) \\ &\quad - I_{c2}Z_e - V_{\pi 2} \end{aligned} \quad (11)$$

$$\begin{aligned} 0 &= sC_{je}V_{\pi 1} + s\tau_F I_{c1} + I_{c1}/\beta_0 + I_{c1} \\ &\quad + sC_{je}V_{\pi 2} + s\tau_F I_{c2} + I_{c2}/\beta_0 + I_{c2}, \end{aligned} \quad (12)$$

respectively, where  $I_{c1}$  and  $I_{c2}$  are collector signal currents (the two collectors are assumed to be ac grounded) of  $Q_1$  and  $Q_2$ , respectively,  $V_{\pi 1}$  and  $V_{\pi 2}$  are signal voltage drops across the base-emitter junctions of  $Q_1$  and  $Q_2$ , respectively. Solving (11) and (12) simultaneously results in the following Volterra series expressions (derivation is shown in Appendix B):

$$\begin{aligned} I_{c1} &= B_1(s) \circ V_s + B_2(s_1, s_2) \circ V_s^2 \\ &\quad + B_3(s_1, s_2, s_3) \circ V_s^3 + \dots \end{aligned} \quad (13)$$

$$\begin{aligned} I_{c2} &= -B_1(s) \circ V_s + B_2(s_1, s_2) \circ V_s^2 \\ &\quad - B_3(s_1, s_2, s_3) \circ V_s^3 + \dots \end{aligned} \quad (14)$$

where  $B_1(s)$  and  $B_2(s_1, s_2)$  are shown in (15) and (16) at the bottom of the page and

$$\begin{aligned} B_3(s_1, s_2, s_3) &= 2B_1(s_1 + s_2 + s_3) \frac{V_T}{3I_T^3} \\ &\quad \times [-B_1(s_1)B_1(s_2)B_1(s_3) + 3I_Q \overline{B_1 B_2}] \\ &\quad \times [1 + (s_1 + s_2 + s_3)C_{je}Z(s_1 + s_2 + s_3)] \end{aligned} \quad (17)$$

$$Z(s) = Z_b(s) + Z_e(s),$$

$$g_m = \frac{I_T}{V_T}.$$

The  $|IM_3|$  (by taking either single-ended or differential output) is given by

$$\begin{aligned} |IM_3| &= \left| \frac{B_1(s)}{I_T} \right|^3 \left| \frac{V_T}{2} [1 + sC_{je}Z(s)] \right. \\ &\quad \times \left[ -1 + \frac{\Delta sC_{je}}{\Delta sC_{je} + \Delta s g_m \tau_F + g_m/\beta_0 + g_m} \right. \\ &\quad \quad \left. + \frac{sC_{je}}{2sC_{je} + 2s g_m \tau_F + g_m/\beta_0 + g_m} \right] \left. \right| \\ &\quad \times |V_s|^2. \end{aligned} \quad (18)$$

The  $|IM_3|$  depends on the magnitude of

$$[1 + sC_{je}Z_b(s) + sC_{je}Z_e(s)],$$

and hence the differential-pair transconductance stage with inductive degeneration is more linear than that with resistive degeneration, which in turn is more linear than that with capacitive degeneration. The  $|IM_3|$  also depends on the magnitude of

$$\begin{aligned} \left[ -1 + \frac{\Delta sC_{je}}{\Delta sC_{je} + \Delta s g_m \tau_F + g_m/\beta_0 + g_m} \right. \\ \left. + \frac{sC_{je}}{2sC_{je} + 2s g_m \tau_F + g_m/\beta_0 + g_m} \right] \end{aligned} \quad (19)$$

where the

$$\left\{ \frac{\Delta sC_{je}}{\Delta sC_{je} + \Delta s g_m \tau_F + g_m/\beta_0 + g_m} + \frac{sC_{je}}{2sC_{je} + 2s g_m \tau_F + g_m/\beta_0 + g_m} \right\}$$

and “-1” terms come from the second-order interaction ( $\overline{B_1 B_2}$ ) and the third-order nonlinearity ( $B_1 B_1 B_1$ ), respectively. The term (19) is independent of the degeneration impedance used, and typically dominated by the third-order nonlinearity. Hence, (18) can be simplified to

$$|IM_3| \approx \left| \frac{B_1(s)}{I_T} \right|^3 \left| \frac{V_T}{2} [1 + sC_{je}Z(s)] \right| |V_s|^2. \quad (20)$$

Comparing (20) with (9) of the common-emitter transconductance stage, we notice that the  $|IM_3|$  of the differential-pair transconductance stage is at least twice as large as that of the common-emitter transconductance stage with the same bias current and transconductance (in this case,  $|A_1(s)/I_Q| = |B_1(s)/I_T|$ ). This condition can only be satisfied when degeneration is used. Without degeneration, common-emitter and differential-pair transconductance stages cannot have the same bias current and transconductance. Without degeneration, we

$$B_1(s) = \frac{g_m}{2[sC_{je}Z(s) + s\tau_F g_m Z(s) + g_m Z(s)/\beta_0 + 1 + g_m Z_e(s)]} \quad (15)$$

$$B_2(s_1, s_2) = B_1(s_1)B_1(s_2) \frac{(s_1 + s_2)C_{je}}{2I_T[(s_1 + s_2)C_{je} + (s_1 + s_2)g_m \tau_F + g_m/\beta_0 + g_m]} \quad (16)$$

have  $0.5|A_1(s)/I_Q| = |B_1(s)/I_T|$ , and hence the  $|IM_3|$  of the common-emitter transconductance stage is twice as large as that of the differential-pair transconductance stage.

### III. CLASS AB BEHAVIOR

The nonlinearity equations derived can be used to explain the class AB behavior described in [3] and [4]. The Volterra series method is effective in predicting distortion in weakly nonlinear conditions such as the small-signal  $IM_3$  distortion (measured by third-order intercept point) which is dominated by the first three Volterra series terms. When larger signals are applied, higher-order terms are needed in the series and the derivation becomes very cumbersome. Nevertheless, the analysis of the weakly nonlinear condition, described in the previous section, can provide insights into class AB behavior (strongly nonlinear condition). However, the analysis does not include terms higher than the third order which are also important in the strongly nonlinear condition.

Gain compression under large-signal conditions is caused by all the odd-order terms in the Volterra series. Assuming that gain compression is dominated by the third-order term, the large-signal transconductance of the common-emitter transconductance stage shown in Fig. 1 can be calculated by using the Volterra series coefficient  $A_3(s_1, s_2, s_3)$  and letting  $s_1 = s, s_2 = s, s_3 = -s$ , where  $s$  is the signal frequency. Hence, the normalized transconductance (normalized to small-signal transconductance) is given by

$$\begin{aligned} |G_M| &= \left| \frac{A_1(s)V_s + \frac{3}{4}A_3(s, s, -s)V_s^3}{A_1(s)V_s} \right| \\ &= \left| 1 + \frac{3}{4} \frac{A_3(s, s, -s)}{A_1(s)} V_s^2 \right| \\ &\approx \left| 1 + A_1^2(s)A_1(-s) \frac{V_T}{4I_Q^3} [1 + sC_{je}Z(s)] \right. \\ &\quad \left. \times \left\{ -1 + \frac{A_1(0)}{g_m} + \frac{A_1(2s)}{2g_m} [1 + 2sC_{je}Z(2s)] \right\} V_s^2 \right|. \end{aligned} \quad (21)$$

Gain compression is caused by

$$\begin{aligned} &A_1^2(s)A_1(-s) \frac{V_T}{4I_Q^3} [1 + sC_{je}Z(s)] \\ &\times \left\{ -1 + \frac{A_1(0)}{g_m} + \frac{A_1(2s)}{2g_m} [1 + 2sC_{je}Z(2s)] \right\} V_s^2 \end{aligned} \quad (22)$$

within which the

$$\left\{ -1 + \frac{A_1(0)}{g_m} + \frac{A_1(2s)}{2g_m} [1 + 2sC_{je}Z(2s)] \right\}$$

term has a negative sign because

$$\left\{ \frac{A_1(0)}{g_m} + \frac{A_1(2s)}{2g_m} [1 + 2sC_{je}Z(2s)] \right\}$$

is typically less than one. With resistive degeneration,  $A_1(s)$

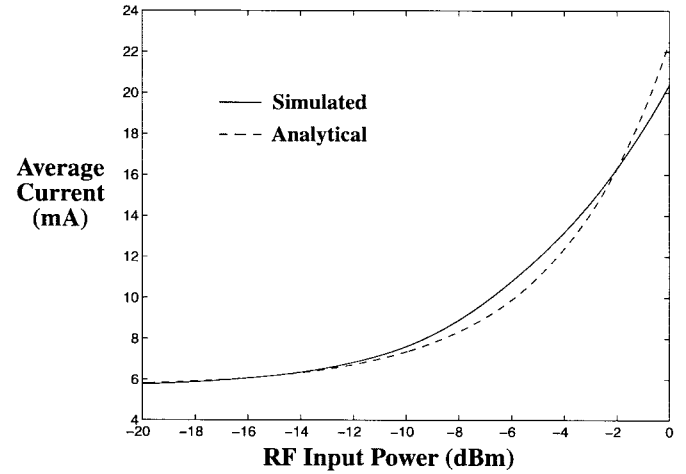


Fig. 8. Average current versus RF input power.

is mostly real, and hence the term (22) is mostly a negative real number which causes gain compression. On the other hand, the term (22) for the inductive degeneration case is a complex number of which the imaginary part is not negligible. As a result, the real part causes gain compression, but the imaginary part causes gain expansion (with phase shift). Although both  $|IM_3|$  and gain compression depends on  $[A_3(s, s, -s)/A_1(s)]$ , the  $|IM_3|$  depends on the magnitude of  $[A_3(s, s, -s)/A_1(s)]$ , whereas the gain compression depends on both magnitude and phase of  $[A_3(s, s, -s)/A_1(s)]$ . Hence, the 1-dB compression point and third-order intercept point are not numerically related at high frequency.

Furthermore, the second-order interaction can be increased to cancel the third-order nonlinearity partially in the inductive degeneration case by increasing the  $[A_1(0)/g_m]$  term. Since this term depends on  $R_1$  as shown in (10),  $R_1$  should be kept small to increase the second-order interaction (to reduce gain compression). In other words,  $R_1$  should be small enough to avoid suppressing the class AB behavior.

Increasing the  $[A_1(0)/g_m]$  term also increases the average current. The increase in average current under large signal condition is caused by all the even-order terms in the Volterra series. Assuming that the increase in average current is dominated by the second-order term, the average current can be calculated by using the Volterra series coefficient  $A_2(s_1, s_2)$  and letting  $s_1 = s, s_2 = -s$ . The magnitude of the average current is given by

$$|I_{ave}| = \left| I_Q + \left[ \frac{1}{2} A_1(0)A_1(s)A_1(-s) \frac{V_T}{2I_Q^2} \right] V_s^2 \right| \quad (23)$$

which depends on the  $A_1(0)$  term. Fig. 8 shows the simulated (using HSPICE) and analytical [using (23)] average current of the common-emitter transconductance stage shown in Fig. 5 as a function of RF input power. As expected, the deviation between the analytical and simulated results increases as the RF input power increases because higher even-order terms in the Volterra series become more significant.

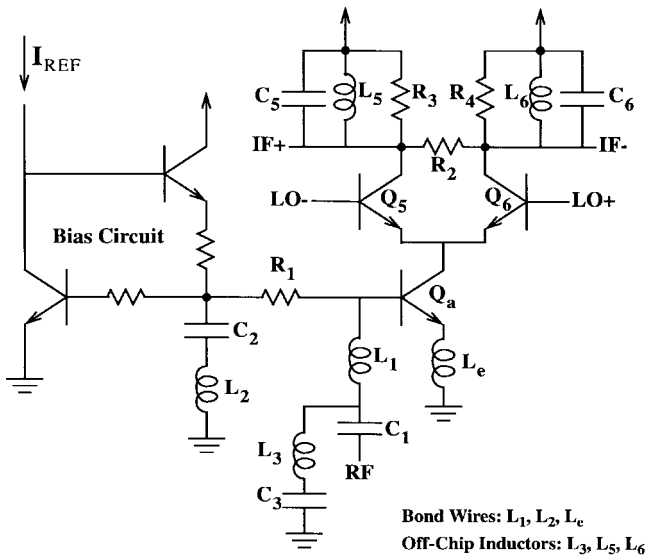


Fig. 9. Class AB mixer.

#### IV. MEASUREMENT RESULTS

Fig. 9 shows the basic circuit topology of the class AB mixer described in [3]. It comprises a common-emitter transconductance stage ( $Q_a$ ) and a differential switching pair ( $Q_5$  and  $Q_6$ ). The design is implemented in a 25-GHz  $f_T$  bipolar process. In this design, the nonlinearity (third-order intermodulation) is dominated by that of the transconductance stage since the switching pair (23-GHz  $f_T$  devices switching at 1.15 GHz LO frequency) can be switched very rapidly. Inductive degeneration (as opposed to resistive degeneration) is used to increase the linearity of the transconductance stage. In order to increase the second-order interaction, the value of  $R_1$  is chosen to be 150  $\Omega$ , which is less than the value of  $r_\pi$  (330  $\Omega$ ) of  $Q_a$ .

The design achieves an input third-order intercept point ( $IP_3$ ) and an input 1-dB compression point ( $P_{-1\text{dB}}$ ) of 2.5 and -1.5 dBm, respectively, at 900 MHz RF frequency. Due to the class AB behavior [3], [4], the numerical difference between the  $P_{-1\text{dB}}$  and  $IP_3$  is different from the commonly known value of 9.6 dB. Simulation (using HSPICE) predicts an input  $IP_3$  of 3.3 dBm. Ignoring the  $IM_3$  contribution from the switching pair, (6) predicts an input  $IP_3$  of 3.6 dBm. Ignoring  $C_\mu$  of  $Q_a$  in the analysis does not introduce significant error. Equation (21) is only used to provide insight into the class AB behavior. It cannot be used to predict the  $P_{-1\text{dB}}$ . Furthermore, the  $P_{-1\text{dB}}$  of this mixer is dominated by saturation at the collectors of the switching pair ( $Q_5$  and  $Q_6$ ). Using a bias current of 5.6 mA, the average currents increase to 6.8 mA and 10.1 mA when RF signals of -10 and -5 dBm are applied to the RF input port, respectively. Equation (23) predicts average currents of 7.3 and 11 mA, respectively.

As a comparison to the above results, if the common-emitter transconductance stage shown above used resistive degeneration instead of inductive degeneration (with the same bias current and transconductance), simulation showed that the input  $IP_3$  would be reduced to 1 dBm. Similarly, if it used

capacitive degeneration, the input  $IP_3$  would be only -2 dBm. On the other hand, the input  $IP_3$  of an inductively degenerated differential-pair transconductance stage (as opposed to the common-emitter transconductance stage described above) with the same current and transconductance would be 0.2 dBm.

#### V. CONCLUSION

Nonlinearity equations in Volterra series for common-emitter and differential-pair transconductance stages have been derived. The equations show that transconductance stages with inductive degeneration have smaller input-referred third-order intermodulation than those with resistive or capacitive degeneration. Second-order interaction, which is stronger in the inductive degeneration case, helps to cancel the third-order nonlinearity. The equations also show that the magnitude of the input-referred third-order intermodulation of the differential-pair transconductance stage is at least twice as large as that of the common-emitter transconductance stage with the same bias current and transconductance (with degeneration). Thus, a common-emitter transconductance stage can be biased at a lower current than a differential-pair transconductance stage with the same linearity and transconductance. Similarly, inductive degeneration is more current efficient than both resistive and capacitive degeneration. The nonlinearity equations can be used to explain the class AB behavior of the common-emitter transconductance stage with inductive degeneration.

#### APPENDIX A

The Kirchhoff's voltage law equation for the common-emitter transconductance stage is

$$V_s = (sC_{je}C_\pi + s\tau_F I_c + I_c/\beta_0)(Z_b + Z_e) + I_c Z_e + V_\pi. \quad (1)$$

Substituting

$$I_c = I_Q \exp\left(\frac{V_\pi}{V_T}\right) = I_Q \left[ \left(\frac{V_\pi}{V_T}\right) + \frac{1}{2}\left(\frac{V_\pi}{V_T}\right)^2 + \frac{1}{6}\left(\frac{V_\pi}{V_T}\right)^3 + \dots \right] \quad (24)$$

and

$$V_\pi = C_1(s_1) \circ V_s + C_2(s_1, s_2) \circ V_s^2 + C_3(s_1, s_2, s_3) \circ V_s^3 + \dots \quad (25)$$

into (1), and solving for  $C_1(s_1)$ ,  $C_2(s_1, s_2)$ , and  $C_3(s_1, s_2, s_3)$  results in

$$C_1(s) = \frac{1}{[sC_{je}Z(s) + s\tau_F g_m Z(s) + g_m Z(s)/\beta_0 + 1 + g_m Z_e(s)]} \quad (26)$$

$$D_1(s) = \frac{1}{2[sC_{je}Z(s) + s\tau_F g_m Z(s) + g_m Z(s)/\beta_0 + 1 + g_m Z_e(s)]}, \quad (36)$$

$$D_2(s_1, s_2) = -D_1(s_1)D_1(s_2) \frac{I_T[(s_1 + s_2)\tau_F + 1/\beta_0 + 1]}{2V_T^2[(s_1 + s_2)C_{je} + (s_1 + s_2)\tau_F g_m + g_m/\beta_0 + g_m]} \quad (37)$$

$$D_3(s_1, s_2, s_3) = -\frac{D_1(s_1 + s_2 + s_3)I_T}{3V_T^3} [D_1(s_1)D_1(s_2)D_1(s_3) + 6V_T \overline{D_1 D_2}] \\ \times \left[ (s_1 + s_2 + s_3)\tau_F Z(s_1 + s_2 + s_3) + \frac{Z(s_1 + s_2 + s_3)}{\beta_0} + Z_e(s_1 + s_2 + s_3) \right]. \quad (38)$$

$$C_2(s_1, s_2) = -C_1(s_1 + s_2)C_1(s_1)C_1(s_2) \frac{I_Q}{2V_T^2} \\ \times \left[ (s_1 + s_2)\tau_F Z(s_1 + s_2) + \frac{Z(s_1 + s_2)}{\beta_0} + Z_e(s_1 + s_2) \right]. \quad (27)$$

$$C_3(s_1, s_2, s_3) = -\frac{A_1(s_1 + s_2 + s_3)I_Q}{6V_T^3} \\ \times [A_1(s_1)A_1(s_2)A_1(s_3) + 6V_T \overline{A_1 A_2}] \\ \times \left[ (s_1 + s_2 + s_3)\tau_F Z(s_1 + s_2 + s_3) + \frac{Z(s_1 + s_2 + s_3)}{\beta_0} + Z_e(s_1 + s_2 + s_3) \right]. \quad (28)$$

Substituting (25) into (24) results in

$$A_1(s) = g_m C_1(s) \quad (29)$$

$$A_2(s_1, s_2) = g_m C_2(s_1, s_2) + \frac{I_Q}{2V_T^2} C_1(s_1)C_1(s_2) \quad (30)$$

$$A_3(s_1, s_2, s_3) = g_m C_3(s_1, s_2, s_3) \\ + \frac{I_Q}{6V_T^3} C_1(s_1)C_1(s_2)C_1(s_3) \\ + \frac{I_Q}{V_T^2} \overline{C_1 C_2}. \quad (31)$$

Equations (3)–(5) can be obtained by expanding (29)–(31), respectively.

## APPENDIX B

The Kirchhoff's voltage and current law equations for the differential-pair transconductance stage are

$$V_s = (sC_{je}V_{\pi 1} + s\tau_F I_{c1} + I_{c1}/\beta_0)(Z_b + Z_e) \\ + I_{c1}Z_e + V_{\pi 1} \\ - (sC_{je}V_{\pi 2} + s\tau_F I_{c2} + I_{c2}/\beta_0)(Z_b + Z_e) \\ - I_{c2}Z_e - V_{\pi 2} \quad (11)$$

$$0 = sC_{je}V_{\pi 1} + s\tau_F I_{c1} + I_{c1}/\beta_0 + I_{c1} \\ + sC_{je}V_{\pi 2} + s\tau_F I_{c2} + I_{c2}/\beta_0 + I_{c2}. \quad (12)$$

Substituting

$$I_{c1} = I_T \left[ \left( \frac{V_{\pi 1}}{V_T} \right) + \frac{1}{2} \left( \frac{V_{\pi 1}}{V_T} \right)^2 + \frac{1}{6} \left( \frac{V_{\pi 1}}{V_T} \right)^3 + \dots \right] \quad (32)$$

$$I_{c2} = I_T \left[ \left( \frac{V_{\pi 2}}{V_T} \right) + \frac{1}{2} \left( \frac{V_{\pi 2}}{V_T} \right)^2 + \frac{1}{6} \left( \frac{V_{\pi 2}}{V_T} \right)^3 + \dots \right] \quad (33)$$

$$V_{\pi 1} = D_1(s_1) \circ V_s + D_2(s_1, s_2) \circ V_s^2 + D_3(s_1, s_2, s_3) \circ V_s^3 + \dots \quad (34)$$

and

$$V_{\pi 2} = -D_1(s_1) \circ V_s + D_2(s_1, s_2) \circ V_s^2 \\ - D_3(s_1, s_2, s_3) \circ V_s^3 + \dots \quad (35)$$

into (11) and (12), and solving for  $D_1(s_1)$ ,  $D_2(s_1, s_2)$ , and  $D_3(s_1, s_2, s_3)$  results as shown in (36)–(38) at the top of the page. Substituting (34) and (35) into (32) and (33), respectively, results in

$$B_1(s) = g_m D_1(s) \quad (39)$$

$$B_2(s_1, s_2) = g_m D_2(s_1, s_2) + \frac{I_T}{2V_T^2} D_1(s_1)D_1(s_2) \quad (40)$$

$$B_3(s_1, s_2, s_3) = g_m D_3(s_1, s_2, s_3) \\ + \frac{I_T}{6V_T^3} D_1(s_1)D_1(s_2)D_1(s_3) \\ + \frac{I_T}{V_T^2} \overline{D_1 D_2}. \quad (41)$$

Equations (15)–(17) can be obtained by expanding (39)–(41), respectively.

## REFERENCES

- [1] D. D. Weiner and J. F. Spina, *Sinusoidal Analysis and Modeling of Weakly Nonlinear Circuits*. New York: Van Nostrand Reinhold, 1980.
- [2] S. A. Mass, *Nonlinear Microwave Circuits*. Norwood, MA: Artech House, 1988.
- [3] K. L. Fong, C. D. Hull, and R. G. Meyer, "A class AB monolithic mixer for 900 MHz applications," *IEEE J. Solid-State Circuits*, vol. 32, pp. 1166–1172, Aug. 1997.
- [4] K. L. Fong and R. G. Meyer, "A 2.4 GHz monolithic mixer for wireless LAN applications," in *IEEE Custom Integrated Circuits Conf.*, May 1997, pp. 9.4.1–9.4.1.

- [5] C. D. Hull, "Analysis and optimization of monolithic RF downconversion receivers," University of California at Berkeley, Berkeley, CA, Ph.D. dissertation, 1992.
- [6] D. O. Pederson and K. Mayaram, *Analog Integrated Circuits for Communication*. Norwell, MA: Kluwer, 1991.



**Keng Leong Fong** (S'93–M'97) was born in Kuala Lumpur, Malaysia, on March 6, 1970. He received the B.A.Sc. degree in engineering science (computer engineering option) and the M.A.Sc. degree in electrical engineering, both from the University of Toronto, Ontario, in 1992 and 1993, respectively. He received the Ph.D. degree in electrical engineering from the University of California at Berkeley in 1997.

During the summer of 1995, he worked at Rockwell International Corporation, Newport Beach, CA, where he was involved in designing class AB mixer and evaluating CAD tools for nonlinear noise analysis. During the summer of 1996, he worked in the same company, designing class AB power amplifiers. Since August 1997, he has been employed by Philips Semiconductors, Sunnyvale, CA. His current research interest is in the area of analog integrated circuit design for RF applications.



**Robert G. Meyer** (S'64–M'68–SM'74–F'81) was born in Melbourne, Australia, on July 21, 1942. He received the B.E., M.Eng.Sci., and Ph.D. degrees in electrical engineering from the University of Melbourne in 1963, 1965, and 1968, respectively.

In 1968, he was employed as an Assistant Lecturer in electrical engineering at the University of Melbourne. Since September 1968, he has been employed in the Department of Electrical Engineering and Computer Sciences, University of California, Berkeley, where he is now a Professor. His current

research interests are high-frequency analog integrated-circuit design and device fabrication. He has acted as a consultant on electronic circuit design for numerous companies in the electronics industry. He is coauthor of the book *Analysis and Design of Analog Integrated Circuits* (Wiley, 1993) and Editor of the book *Integrated Circuit Operational Amplifiers* (IEEE Press, 1978).

Dr. Meyer was President of the IEEE Solid-State Circuits Council and was an Associate Editor of the IEEE JOURNAL OF SOLID-STATE CIRCUITS and of the IEEE TRANSACTIONS ON CIRCUITS AND SYSTEMS.